Efficient Quantum Transduction Using Anti-Ferromagnetic Topological Insulators

Haowei Xu[1], Changhao Li[1,2], Guoqing Wang[1,2], Hao Tang[3],

Paola Cappellaro[1,2,4, †], and Ju Li[1,3, ‡]

[1] Department of Nuclear Science and Engineering, Massachusetts Institute of Technology, Cambridge, Massachusetts 02139, USA

[2] Research Laboratory of Electronics, Massachusetts Institute of Technology, Cambridge, MA 02139, USA

[3] Department of Materials Science and Engineering, Massachusetts Institute of Technology, Cambridge, Massachusetts 02139, USA

[4] Department of Physics, Massachusetts Institute of Technology, Cambridge, MA 02139, USA

* Corresponding authors: † pcappell@mit.edu, ‡ liju@mit.edu

Abstract

Transduction of quantum information between distinct quantum systems is an essential step in various applications, including quantum networks and quantum computing. However, quantum transduction needs to mediate between photons with vastly different frequencies, making it challenging to design high-performance transducers, due to multifaceted and sometimes conflicting requirements. In this work, we first discuss some general principles for quantum transducer design, and then propose solid-state anti-ferromagnetic topological insulators to serve as highly effective transducers. First, topological insulators exhibit band-inversion, which can greatly enhance their optical responses. Coupled with their robust spin-orbit coupling and high spin density, this property leads to strong nonlinear interaction in topological insulators, thereby substantially improving transduction efficiency. Second, the anti-ferromagnetic order can minimize the detrimental influence on other neighboring quantum systems due to magnetic interactions. Using $MnBi_2Te_4$ as an example, we showcase that unit transduction fidelity can be achieved with modest experimental requirements, while the transduction bandwidth can reach the GHz range. The strong nonlinear interaction in magnetic topological insulators can find diverse applications, including the generation of entanglement between photons of distinct frequencies.

Introduction. Quantum information processing systems typically operate in distinct frequency domains. For example, quantum processors such as superconducting qubits, one of the leading platforms in quantum computation, work at microwave (MW) frequencies. Meanwhile, photons with infrared (IR) to visible frequencies can serve as flying qubits for long-distance communication. Therefore, efficient quantum transduction between different frequency domains is crucial to harness the advantages of different platforms in hybridized quantum systems and quantum networks.

We will specifically focus on the transduction between MW and IR photons. An ideal quantum transducer should exhibit strong interaction with both MW and IR photons, so that high transduction efficiency and bandwidth can be enabled. Meanwhile, it is also necessary to minimize any adverse influence on the quantum system (e.g., superconducting qubits) resulting from the coupling with the transducer. Diverse transduction schemes have been explored, involving e.g., neutral atoms [1,2], rare-earth-doped crystals [3,4], optomechanical devices [5–7], electro-optics [6–8], and magnons [9,10]. Unfortunately, it is a nontrivial task to identify a high-performance transducer. For example, while Rydberg atoms have relatively strong interaction with MW photons, their large polarizabilities can also lead to decoherence and even destroy the superconducting states of superconducting qubits [11,12]. Electro-optical devices, on the other hand, suffer from weak nonlinearities below 10^3 pm/V [13].

Magnetic topological insulators (MTIs) [14–17] are a class of magnetic materials with nontrivial electronic band topology, which have attracted wide interest in condensed matter physics. In MTIs, the combination of the nontrivial electronic band topology and magnetism leads to a wealth of novel properties, such as the quantum anomalous Hall effect [16] and axion electrodynamics [17]. These unique properties suggest novel applications of MTIs. In this work, we propose that MTIs, particularly anti-ferromagnetic topological insulators (AFMTIs), hold great potential in quantum information science as well, thanks to their enhanced linear and nonlinear optical response. Specifically, we will demonstrate that AFMTI can serve as efficient quantum transducers, which could enable unit transduction fidelity and wide bandwidth exceeding GHz. Regarding transduction applications, the inherent collective spin excitation (magnon) frequencies in magnetic materials typically fall in the MW range [18–20]. Considering the ultra-large number density ($\sim 10^{28}$ m^{-3}) of magnetic moments, this suggests that magnetic materials can have strong coupling with MW photons [9,10]. Additionally, if anti-ferromagnetic (AFM) materials are used as the transducer, the influence on nearby

quantum systems can be minimized, because AFM materials have vanishing total magnetic moments. Indeed, these features have elicited great interest in AFM spintronics [18,19].

Moreover, the nontrivial electronic band topology of MTIs can greatly boost the quantum transduction performance. Topological insulators feature band inversion [21,22], whereby the energy ordering of normal valence and conduction bands is inverted in certain regions of the Brillouin zone. The band inversion usually leads to stronger hybridization between valence and conduction band wavefunctions, which in turn results in larger Berry curvature and stronger coupling with visible and IR photons [23–26]. Meanwhile, topological insulators typically possess heavy elements and thus strong spin-orbit coupling (SOC), which accelerates the conversion between spin and orbital dynamics and further improves the transduction efficiency in MTIs. Synergistically, these features contribute to the proposed performance of MTI quantum transducers.

In the following, we will first discuss some general principles to improve transduction efficiency. Then, we will introduce the mechanism of quantum transduction in magnetic materials and explain why AFMTIs can be efficient transducers. Using $MnBi_2Te_4$ [27–29] as an example, we will demonstrate the enhanced coupling strength with MW and IR photons in AFMTIs. We will show that the quantum transduction using $MnBi_2Te_4$ as the transducer can achieve unit transduction fidelity with modest experimental requirements. The bandwidth of the transduction can potentially reach GHz, nearly two orders of magnitude larger than the typical bandwidth based on other transduction schemes [30]. The intrinsic second-order $\chi^{(2)}$ nonlinearity of $MnBi_2Te_4$ can reach 10^6 pm/V, orders of magnitude larger than that of typical electro-optical materials [13] and topologically trivial magnetic materials [9,10]. Besides, the transduction scheme we proposed is applicable in centrosymmetric materials, in contrast to the electro-optical effect, which requires inversion symmetry breaking.

Design principles for efficient transducers. The purpose of the transduction process is to convert MW photons to IR photons (or vice versa), whose frequencies are ω_{MW} and ω_{IR}, respectively. A pumping laser with a frequency $\omega_{\mathrm{pump}} = \omega_{\mathrm{IR}} - \omega_{\mathrm{MW}}$ is applied, so that energy conservation can be satisfied. To achieve efficient quantum transduction, the transducer should have strong coupling with both MW and IR photons, which have drastically different frequencies. Establishing strong coupling between quantum degrees of freedom (DoF) generally requires resonance (frequency matching) conditions. However, a single DoF cannot be resonant with two vastly different frequencies simultaneously. Actually, this leads to an intrinsic limit on the coupling strength of the electro-optical effect from pure electronic

responses [31], whereby the MW and the IR/visible photons are both coupled to the electronic orbital transitions (~ 1 eV) in semiconductors. The MW photons (~ 0.1 meV) are far off-resonance, leading to weak responses. Indeed, in materials with soft phonon modes, such as $BaTiO_3$ [32,33], the major contribution to the electro-optical responses comes from ionic (i.e., phonon) responses [13], whereby the detuning between phonons and MW photons can be relatively smaller.

A potentially better strategy is to employ a transducer with two DoFs designed to be (nearly) resonant with MW and IR photons, respectively. These two DoFs are then coupled by a specific internal interaction within the transducer. For example, using Rydberg atoms, the MW photons are coupled with the transitions between two highly excited Rydberg states. By judiciously selecting the principal quantum numbers of the Rydberg states, nearly resonant conditions can be satisfied, which can significantly improve the coupling strength. Unfortunately, this also leads to some detrimental effects, such as large polarizabilities [30].

On the other hand, the transduction scheme based on rare-earth-ion doped crystals [3,4] or magnons [9,10] utilizes the two intrinsic DoFs of electrons, namely spin and orbital excitations, which are internally coupled by the spin-orbit coupling (SOC) ubiquitous in atoms, molecules, and solid-state systems. The orbital excitation energy of electrons is usually on the order of 1 eV, facilitating the coupling with photons in the visible or IR range. To utilize the spin DoF, it is necessary to have unpaired electron spins (magnetic moments), which can result from dopants, such as rare-earth-ions, in crystals. In terms of coupling strength, a more favorable option is to use pristine magnetic materials [9,10], where the number density of electron magnetic moments can reach 10^{28} m^{-3}. Besides, it is not necessary to use external magnetic fields to sustain the spin splitting in magnetic materials, which can be advantageous as well. In ferromagnetic materials, the spin excitation (magnon) frequency ω_m is typically on the order of GHz and is close to MW frequencies, but the macroscopic magnetic moments and the resultant magnetic fields can adversely affect the performance of the quantum objects (e.g., superconducting qubits) adjacent to the transducer [9,10].

In this regard, we suggest using AFM materials, whose net macroscopic magnetic moment is zero. However, a potential concern arises from the high magnon frequencies ω_m in AFM materials (up to the THz range [18,19]), which can lead to relatively large detuning from the frequencies of MW photons. Therefore, soft AFM materials with relatively low magnon frequencies (down to 100 GHz) would be more favorable. Furthermore, it is crucial to establish

a general approach for selecting or designing AFM materials that can strongly interact with IR and/or MW photons, so that the overall transduction efficiency can be improved.

The discussions above lead us to the proposal of using AFMTIs as the transducer. As we will explain in more detail later, compared with topologically trivial AFM materials, AFMTIs have enhanced coupling strength with IR photons, thanks to their band inversion. AFMTIs also possess strong intrinsic SOC, resulting in rapid conversion between spin and orbital dynamics, which is beneficial for quantum transduction. Consequently, the transduction efficiency can be strong despite the relatively large frequency detuning between AFM magnons and MW photons. In the following, we will argue that AFMITs can potentially serve as efficient quantum transducers, and their transduction performance can be orders of magnitude better than trivial AFM materials such as Cr_2O_3.

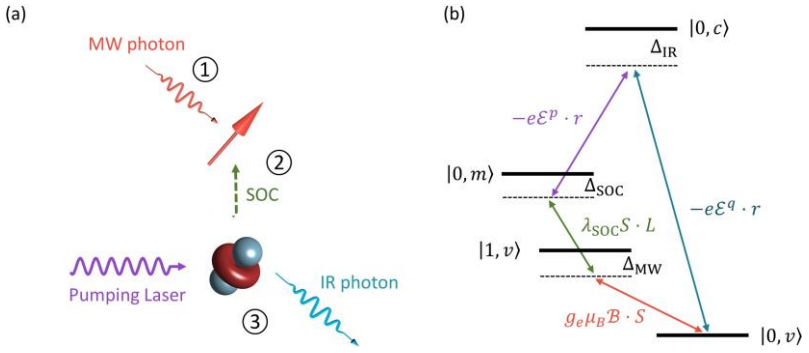

Figure 1. Schematic diagram showing the mechanism of the transduction based on MTIs (the MW→IR process). MW and IR photons interact with the spin and orbital degrees of freedom of the electrons, respectively, which are internally coupled by SOC. A pumping laser is applied so that energy conservation can be fulfilled. (b) Energy level diagram of the transduction process.

Transduction mechanism in anti-ferromagnetic materials. We first examine the mechanism of transduction using AFM materials. Although magnons in AFM materials are collective spin excitations, for the sake of simplicity, we will treat every unit cell individually. This approach is valid since photons only interact with magnons with wavevectors $\boldsymbol{k} \approx 0$. SOC will only be considered for the interconversion between spin and orbital dynamics and will be disregarded elsewhere. The quantum state of electrons can be labeled with $|\mathcal{N}, m\rangle$, where the electron wavevector $\boldsymbol{k}$ is omitted, $\mathcal{N} = 0,1,2,\ldots$ denotes the number of magnons, while m denotes the orbital state of the electrons. The energy of $|\mathcal{N}, m\rangle$ is labeled as $E_{|\mathcal{N},m\rangle}$. We assume the electron is initially on the $|0, v\rangle$ state with v a valence state. The electron, as the transducer,

shall return to this initial state after the whole transduction is finished. Note that the localized magnetic moment in magnetic materials mostly comes from the electron spins, instead of orbital angular momenta [34]. We will thus use spin and magnetic moment interchangeably hereafter.

To facilitate further discussions, we separate the transduction process into three steps (Figure 1a). First, the magnetic field $\mathcal{B}$ of the MW photon interacts with the electron spin S through the Zeeman interaction $H_{\mathrm{Z}} = g_{\mathrm{e}}\mu_{\mathrm{B}} S \cdot \mathcal{B}$, where g_{e} is the electron g-factor and μ_{B} is the Bohr magneton. Due to the Zeeman interaction, one magnon can be excited and the electron thus jumps to the $|1, v\rangle$ state. The strength of this first step can be obtained from perturbation theory, and can be characterized by $\xi_{\mathrm{MW}} = \frac{\langle 0,v|H_Z|1,v\rangle}{\Delta_{\mathrm{MW}}}$, where $\Delta_{\mathrm{MW}} \equiv E_{|1,v\rangle} - E_{|0,v\rangle} - \omega_{\mathrm{MW}} = \omega_m - \omega_{\mathrm{MW}}$ is the frequency mismatch between the MW photon and the magnon. Note that in practice Δ_{MW} should be large enough to avoid the resonant absorption of the MW photon by magnons, which is undesirable for transduction.

Next, SOC induces a $|1, v\rangle \rightarrow |0, m\rangle$ transition, whereby the electron spin DoF returns to the ground state ($\mathcal{N} = 0$), while the orbital DoF transits from $|v\rangle$ to an intermediate state $|m\rangle$. The strength of this second step is characterized by $\xi_{\mathrm{SOC}} = \frac{\langle 1,v|H_{\mathrm{SOC}}|0,m\rangle}{\Delta_{\mathrm{SOC}}}$, where $H_{\mathrm{SOC}} = \lambda_{\mathrm{SOC}} S \cdot L$ is the SOC Hamiltonian, λ_{SOC} is the SOC strength, L is the angular momentum operator, while $\Delta_{\mathrm{SOC}} \equiv E_{|0,m\rangle} - E_{|1,v\rangle} - \omega_{\mathrm{MW}}$ is the energy detuning. Here the SOC is considered a static interaction. Generally, the numerator $\langle 1, v|H_{\mathrm{SOC}}|0, m\rangle$ has a similar order of magnitude for all possible m. Hence, ξ_{SOC} can be maximized when Δ_{SOC} is minimized. This condition is satisfied when $m = v$, whereby one has $\Delta_{\mathrm{SOC}} \sim 100\ \mathrm{GHz} \sim 1\ \mathrm{meV}$, corresponding to MW frequencies, otherwise one usually has $\Delta_{\mathrm{SOC}} \sim 1\ \mathrm{eV}$ for $m \neq v$.

During the third step of the transduction process, two IR fields p and q interact with the electron orbital motion via the electric dipole interaction $H_{\mathrm{d}}^{p\,(q)} = -e\mathcal{E}^{p\,(q)} \cdot r$, where r is the electron position operator, and $\mathcal{E}^{p\,(q)}$ is the IR electric field. For definiteness, the p and q fields will hereafter correspond to the pumping laser and the transduced IR photon, respectively (Figure 1). Specifically, the $|0, m\rangle$ electron jumps to another intermediate state $|0, c\rangle$ via H_{d}^{p}, whereby a p-photon is absorbed, and then returns to the initial state $|0, v\rangle$ via H_{d}^{q}, whereby a q-photon is emitted. The strength of this two-photon process can be characterized by $\xi_{\mathrm{IR}} = \sum_c \frac{\langle 0,m|H_{\mathrm{d}}^{p}|0,c\rangle\langle 0,c|H_{\mathrm{d}}^{q}|0,v\rangle}{\Delta_{\mathrm{IR}}}$ with $\Delta_{\mathrm{IR}} \equiv E_{|0,c\rangle} - E_{|0,v\rangle} - \omega_{\mathrm{IR}}$, where ω_{IR}

is the frequency of the q-photon. But to the leading order of the analysis, we can also take ω_{IR} to be the frequency of the p-photon due to the small frequency difference between the two IR fields.

Altogether, the MW to IR transduction process is: (1) incident MW photons (virtually) excite magnons (spin excitations); (2) the spin excitations are converted to orbital excitations through SOC; (3) following the laser-pumped transitions, the orbital excitations decay, resulting the emission of IR photons (Figure 1). In principle, these three steps have equal status and can occur simultaneously. The separation into three steps should be regarded as artificial, which leads to the fact that ξ_{MW} and ξ_{SOC} are unitless, while ξ_{IR} has a unit of energy. A more rigorous treatment can be formulated using third-order perturbation theory [35]. The overall coupling strength of the transduction can be expressed as [see Supplementary Materials (SM) for details]

$$\mathcal{G} \approx \frac{N_{\mathrm{s}} g_{\mathrm{e}} \mu_{\mathrm{B}} S\, \mathcal{B} \cdot \lambda_{\mathrm{SOC}} \cdot \varepsilon_0 \chi_r(\omega_{\mathrm{IR}}) V_{\mathrm{cell}} \mathcal{E}^p \mathcal{E}^q}{\Delta_{\mathrm{MW}} \Delta_{\mathrm{SOC}}} \tag{1}$$

Here N_{s} and V_{cell} are the total number of magnetic moments and the volume of the unit cell. Note that in AFM materials, the magnetic moments are fully concentrated, and one has $N_{\mathrm{s}} V_{\mathrm{cell}} \sim V_0$ with V_0 the volume of the crystal. Meanwhile, ε_0 and $\chi_r(\omega_{\mathrm{IR}})$ are the vacuum permittivity and the optical susceptibility of the host material, respectively. From Eq. (1), one can observe that the coupling strength $\mathcal{G}$ is determined by the product of the strength of the three steps, which are represented by $N_s g_{\mathrm{e}} \mu_{\mathrm{B}} S\mathcal{B}$, λ_{SOC}, and $\varepsilon_0 \chi_r(\omega_{\mathrm{IR}}) V_0 \mathcal{E}^p \mathcal{E}^q$, respectively. In addition, $\mathcal{G}$ is also influenced by Δ_{MW} and Δ_{SOC}. For AFM magnons, one typically has $\Delta_{\mathrm{MW\,(SOC)}} \gtrsim 100\ \mathrm{GHz}$, which is well above the magnon linewidth [18,19]. Δ_{MW} and Δ_{SOC} can potentially be reduced by applying externally static magnetic fields $\mathcal{B}_0$, which modulate magnon frequencies. Fortunately, $\mathcal{G}$ is sufficiently strong even if $\mathcal{B}_0 = 0$, as demonstrated later.

Additionally, we would like to remark that the transduction scheme described above can be used in centrosymmetric materials. Specifically, under spatial inversion operation, $\mathcal{G} \sim \mathcal{B}\mathcal{E}^2$ in Eq. (1) is invariant, as $\mathcal{B}$ and $\mathcal{E}$ get a $+1$ and -1 sign, respectively. In comparison, the electro-optical effect requires inversion symmetry breaking, because its coupling strength $\mathcal{G}_{\mathrm{EO}} \sim \mathcal{E}^3$ undergoes a sign change under spatial inversion, hence it must be zero in centrosymmetric materials.

Enhanced coupling strength in material topological insulators. To improve the transduction performance, it is essential to enhance $\mathcal{G}$. This involves optimizing each of the three steps described above. Typically, the electron g-factor is close to 2 in magnetic materials [34,36–39]. Hence, to improve the strength of the first step (Zeeman interaction), one has to increase the number of electron spins N_s. This emphasizes the advantage of using magnetic materials, where the magnetic moments are fully concentrated [10], resulting in large N_s.

In contrast, the strengths of the second and third steps, which are determined by the SOC strength λ_{SOC} and the optical susceptibility $\chi_r(\omega_{IR})$, can vary significantly in different materials. Notably, λ_{SOC} and $\chi_r(\omega_{IR})$ in many scenarios are independent of each other. A strong SOC does not necessarily indicate strong optical responses, and vice versa [40]. Actually, some materials possessing strong optical responses, such as graphene [41] or MoS_2 [42], have weak SOC. Is there a systematic strategy to improve λ_{SOC} and $\chi_r(\omega_{IR})$ simultaneously? MTIs [14,15] provide a viable solution. Strong SOC is usually a necessary condition for non-trivial electronic band topology, and thus topological insulators possess heavy elements and strong SOC [21,22]. Meanwhile, the electronic band inversion in topological insulators leads to significant wavefunction hybridization between the valence and conduction bands. This results in faster interband transition rates and thus stronger bulk optical responses [23–25], which has been verified experimentally [26].

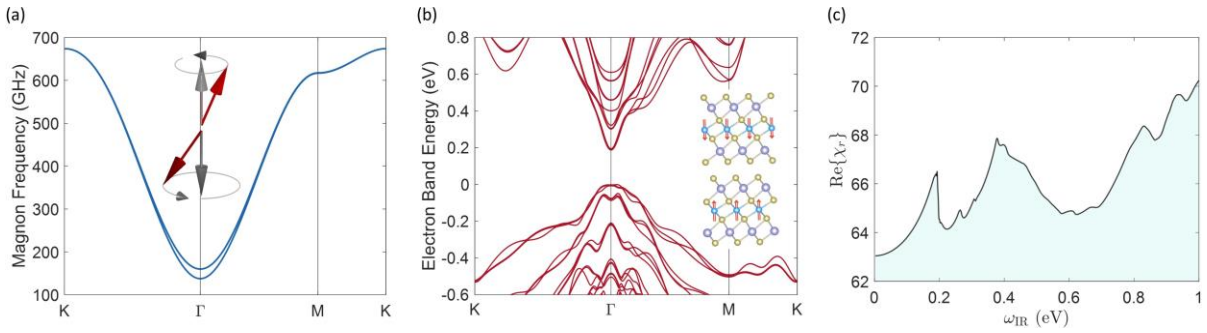

Figure 2. (a) Magnon dispersion of $MnBi_2Te_4$. Inset shows the spin precession in AFM materials when magnons are excited. Spins (red arrows) precess around the ground state (grey arrows, no magnons). (b) Electron band structure of $MnBi_2Te_4$. Inset shows the atomic structure of $MnBi_2Te_4$. Blue: Mn; Purple: Bi; Brown: Te. The arrows on Mn atoms indicate the magnetic moments with AFM configuration. (c) The real part of the optical susceptibility of $MnBi_2Te_4$.

Next, we will use $MnBi_2Te_4$ [27–29] as an example to demonstrate the potential of MTIs as quantum transducers. $MnBi_2Te_4$ has a layered structure (inset of Figure 2b), and on each layer, magnetic Mn atoms are sandwiched by Bi and Te atoms in the sequence of Te–Bi–Te–Mn–Te–Bi–Te. A minimal Hamiltonian for the local magnetic momentum ($S = 5/2$) of Mn atoms is [38,43]

$$\mathcal{H}_s = J_1 \sum_{\langle ij \rangle} \boldsymbol{S}_i \cdot \boldsymbol{S}_j + J_c \sum_{\langle ij \rangle'} \boldsymbol{S}_i \cdot \boldsymbol{S}_j + D_z \sum_i (S_i^z)^2 + \gamma_e \sum_i \boldsymbol{\mathcal{B}} \cdot \boldsymbol{S}_i. \tag{2}$$

Here i, j label the Mn atoms, while $\langle ij \rangle$ and $\langle ij \rangle'$ indicate intra- and inter-layer nearest neighbors with spin-spin coupling strength $J_1 = -0.23\ \text{meV}$ and $J_c = 0.065\ \text{meV}$, respectively [38,43]. $D_z = -0.15\ \text{meV}$ characterizes the easy-axis magnetic anisotropy along z axis. With external magnetic field $\mathcal{B} = 0$, the intralayer exchange coupling between Mn atoms is ferromagnetic, while different layers are stacked with an AFM order. The magnon band structure obtained by linearizing Eq. (2) is shown in Figure 2a. The magnon frequency at the Γ-point is $\omega_m \approx 150\ \text{GHz}$, which is relatively low among AFM materials. This is advantageous compared with other AFM materials, since the detuning Δ_{MW} would be smaller for $\omega_{\text{MW}} \sim 10\ \text{GHz}$.

While Mn atoms provide the magnetic moments, the heavy elements Bi and Te contribute to strong SOC in $MnBi_2Te_4$. According to our *ab initio* calculations, the SOC strength relevant to the transduction process is $\lambda_{\text{SOC}} \sim 47\ \text{meV}$ in $MnBi_2Te_4$. As a comparison, the SOC strength in Cr_2O_3 [44], another prototypical AFM insulator, is only around $4\ \text{meV}$, since both Cr and O are light elements. This clearly demonstrates the advantage of using $MnBi_2Te_4$ for transduction. We will use $\lambda_{\text{SOC}} = 10\ \text{meV}$ for $MnBi_2Te_4$ in the following as a conservative estimation.

The strong SOC in $MnBi_2Te_4$ also leads to band inversion and nontrivial topology [27–29]. The electronic band structure of $MnBi_2Te_4$ is shown in Figure 2b. The inverted bandgap at the Γ point is around 0.2 eV, which falls in the mid-infrared range. The optical responses of $MnBi_2Te_4$ have been studied before [17,45–47]. Here we focus on the optical susceptibility $\chi_r(\omega_{\text{IR}})$, which can be expressed as

$$\chi_r(\omega_{\text{IR}}) = \frac{e^2}{\varepsilon_0} \int_k \frac{d\boldsymbol{k}}{(2\pi)^3} \sum_{c,v} \frac{|\langle 0, v|r|0, c\rangle|^2}{E_{|c,0\rangle} - E_{|v,0\rangle} - \omega_{\text{IR}}}, \tag{3}$$

where $\int d\boldsymbol{k}$ indicates the integration in the first Brillouin zone, while $c\,(v)$ indicates conduction (valence) bands. One can see that the magnitude of the numerator, $|\langle 0,v|r|0,c\rangle|^2$, strongly depends on the wavefunction overlap between valence and conduction bands, which is enhanced in topological materials because of the band inversion [23]. The calculated $\chi_r(\omega_{\mathrm{IR}})$ of $MnBi_2Te_4$ is shown in Figure 3c, where one can see that $\chi_r(\omega_{\mathrm{IR}} \to 0)$ is greater than 60, significantly larger than those of typical topologically trivial insulators. As an example, χ_r is below 15 in Cr_2O_3 for below bandgap frequencies (SM Figure S1). This corroborates the enhanced bulk optical responses in topological insulators [23–26].

Here we can compare the coupling strength $\mathcal{G}$ in MBT with that of the electro-optical effect. Converting $\mathcal{B}$ to $\mathcal{E}$ using $\mathcal{B} = \mathcal{E}/c_0$ with c_0 the speed of light, one has $\mathcal{G} \sim \chi^{(2)}_{\mathrm{eff}} V_0 \varepsilon_0 \mathcal{E}^3$, where the effective second-order susceptibility is $\chi^{(2)}_{\mathrm{eff}} \gtrsim 10^6\ \mathrm{pm/V}$ in $MnBi_2Te_4$ when $\Delta_{\mathrm{MW}} = \Delta_{\mathrm{SOC}} = 100\ \mathrm{GHz}$. As a comparison, in electro-optical materials, the second-order susceptibility is typically below $10^3\ \mathrm{pm/V}$ [13]. The large intrinsic nonlinearities also indicate that MTIs can be efficient in other applications besides quantum transduction, such as two-mode squeezing [48] and entanglement generation [49,50].

Quantum transduction using $MnBi_2Te_4$ transducer. In the following, we will explore quantum transduction using $MnBi_2Te_4$ as the transducer. The goal is to achieve efficient conversion between single MW and IR photons. Hence, we consider a setup where the $MnBi_2Te_4$ sample is coupled to both an IR cavity and an MW cavity. Additionally, a classical IR pumping laser with a frequency ω_{pump} is employed so that the frequency-matching condition ($\omega_{\mathrm{MW}} + \omega_{\mathrm{pump}} = \omega_{\mathrm{IR}}$) can be satisfied. Accordingly, we second quantize the magnetic field $\mathcal{B}$ and electric field $\mathcal{E}^q$, and treat $\mathcal{E}^p$ as the classical pumping field in Eq. (1). The quantum transduction process can be described by the beam-splitter Hamiltonian

$$\begin{aligned} \mathcal{H} &= \mathcal{G}\left(a^\dagger_{\mathrm{MW}} a_{\mathrm{IR}} + a^\dagger_{\mathrm{IR}} a_{\mathrm{MW}}\right), \\ \mathcal{G} &= g V_0 \mathcal{B}^{\mathrm{zpf}}_{\mathrm{MW}} \mathcal{E}^{\mathrm{zpf}}_{\mathrm{IR}} \mathcal{E}_{\mathrm{pump}}. \end{aligned} \tag{4}$$

Here $a^\dagger_{\mathrm{MW\,(IR)}}$ is the creation operator for the MW (IR) photon, and $a_{\mathrm{MW\,(IR)}}$ is the corresponding annihilation operator. The collective coupling strength $\mathcal{G}$ is rewritten from Eq. (1). Here $g \equiv \frac{g_e \mu_B \mathcal{S}\cdot\lambda_{\mathrm{SOC}}\cdot\varepsilon_0\chi_r(\omega_{\mathrm{IR}})}{\Delta_{\mathrm{MW}}\Delta_{\mathrm{SOC}}}$ is a reduced coupling strength, $\mathcal{E}_{\mathrm{pump}}$ is the pumping field, while $\mathcal{B}^{\mathrm{zpf}}_{\mathrm{MW}} \equiv \sqrt{\frac{\mu_0\omega_{\mathrm{MW}}}{2V_{\mathrm{MW}}}}$ and $\mathcal{E}^{\mathrm{zpf}}_{\mathrm{IR}} \equiv \sqrt{\frac{\omega_{\mathrm{IR}}}{2\varepsilon_0(\chi_r+1)V_{\mathrm{IR}}}}$ are the zero-point magnetic and electric fields of the MW and IR cavities, respectively. V_{MW} and V_{IR} are the mode volumes of the

cavities. We assume that the $MnBi_2Te_4$ sample fills the IR cavity, and the filling factor $\varphi \sim \frac{V_0}{\sqrt{V_{MW}V_{IR}}}$ can reach 3×10^{-3} when $V_{MW} = 1\ mm^3$ and $V_0 = V_{IR} = 10^4\ \mu m^3$. Note that φ can potentially be even greater, since $MnBi_2Te_4$ samples with larger sizes [29] and MW cavities with smaller mode volumes [51] have been fabricated before. We also take $\omega_{MW} = 10$ GHz, $\omega_{IR} = 0.1$ eV, and $\Delta_{MW} = \Delta_{SOC} = 100$ GHz, which leads to $\mathcal{G}[\text{GHz}] \approx 0.16 \times \mathcal{E}_{pump}[\text{MV} \cdot \text{m}^{-1}]$. Converting $\mathcal{E}_{pump}$ to the number of pumping photons in the cavity n_{pump}, one has $\mathcal{G}[\text{GHz}] \approx 10^{-5} \times \sqrt{n_{pump}}$ under the current settings, which is significantly stronger than the coupling strength in e.g., optomechanics-based transduction [6,7].

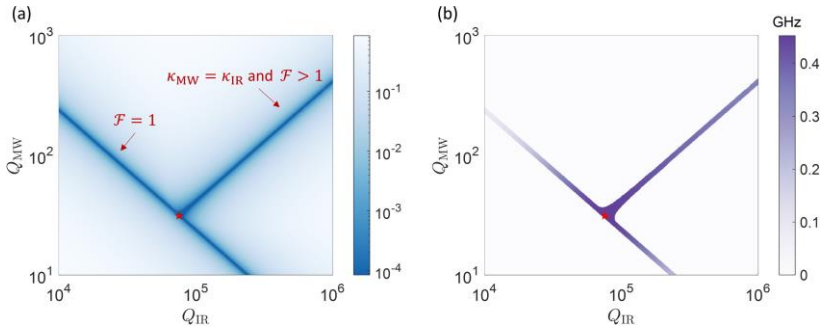

Figure 3. (a) Infidelity $1 - \eta$ and (b) bandwidth f_B [in GHz] of the quantum transduction process as a function of Q_{MW} and Q_{IR}. Stars indicate the optimal setting (impedance matching) whereby the transduction fidelity is unity, and the bandwidth is maximized. In (b), the bandwidth is shown only when $\eta > 1 - 10^{-3}$.

The quantum transduction fidelity η can be estimated from the input-output relations and can be expressed as [3,52,53]

$$\eta(\delta) = \left| \frac{4i\mathcal{G}\sqrt{\kappa_{MW}\kappa_{IR}}}{4\mathcal{G}^2 + (\kappa_{MW} - 2i\delta)(\kappa_{IR} - 2i\delta)} \right|^2 . \quad (5)$$

Here $\delta \equiv \omega_{MW} + \omega_{pump} - \omega_{IR}$ is the detuning from frequency matching condition, while $\kappa_{MW\,(IR)}$ is the linewidth of the MW (IR) cavity.

We first fix $\mathcal{G} = 0.16$ GHz, which can be realized in $MnBi_2Te_4$ using a relatively mild pumping field $\mathcal{E}_{pump} = 1\ \text{MV} \cdot \text{m}^{-1}$ (laser intensity $\sim 1.3\ \text{mW} \cdot \mu\text{m}^{-2}$). The maximum transduction fidelity and full width at half maximum (FWHM) bandwidth are shown in Figure 3, where we vary the quality factors of the MW and IR cavities [$Q_{MW\,(IR)} \equiv \frac{\omega_{MW\,(IR)}}{\kappa_{MW\,(IR)}}$]. Unit transduction

fidelity can be achieved with either $\mathcal{F} = 1$ or $\kappa_{\mathrm{MW}} = \kappa_{\mathrm{IR}}$ and $\mathcal{F} > 1$. Here $\mathcal{F} = \frac{2\mathcal{G}}{\sqrt{\kappa_{\mathrm{MW}}\kappa_{\mathrm{IR}}}}$ is the impedance matching parameter. Meanwhile, the FWHM bandwidth f_{B} can be maximized when $\mathcal{F} = 1$ and $\kappa_{\mathrm{MW}} = \kappa_{\mathrm{IR}}$. This requires $\kappa_{\mathrm{MW}} = \kappa_{\mathrm{IR}} = 0.32$ GHz, corresponding to $Q_{\mathrm{MW}}^{0} \approx 30$ and $Q_{\mathrm{IR}}^{0} \approx 7.5 \times 10^{4}$ (stars in Figure 3), which are well below the highest quality factor achievable [54,55]. The resultant FWHM bandwidth is $f_{\mathrm{B}} = 2\sqrt{2}\mathcal{G} \approx 0.45$ GHz. Note that f_{B} can reach GHz when $\mathcal{E}_{\mathrm{pump}} \gtrsim 2\ \mathrm{MV \cdot m^{-1}}$. This should be compared with the bandwidth of quantum transduction based on other schemes, which is usually below $1 \sim 10$ MHz [1,9,10,30,56,57].

One can see that the key to simultaneously improving the transduction fidelity and FWHM bandwidth is to have large coupling strength $\mathcal{G}$. This highlights the advantage of using MTIs. As a comparison, under the same setting, $\mathcal{G}$ would be smaller by around two orders of magnitude if topologically trivial magnetic materials such as Cr_2O_3 are used as the transducer. This indicates that higher pumping fields ($\sim 100\ \mathrm{MW \cdot m^{-1}}$) are necessary, otherwise MW and IR cavities with smaller linewidths should be used for unity transduction fidelity, whereby the FWHM bandwidth would be lowered to $1 \sim 10$ MHz [30].

Until now, we considered quantum transduction to exemplify the potential of MTIs in quantum engineering. More broadly, MTIs can be advantageous in many other applications that require strong linear or nonlinear optical responses, such as quantum squeezing [48], entanglement generation [49,50], spontaneous parametric down-conversion [58], etc. Furthermore, $MnBi_2Te_4$ can be thinned down to single or multiple layers [27], leading to the possibility of quantum applications that extend to the two-dimensional limit [59].

In conclusion, we proposed that MTIs such as $MnBi_2Te_4$ can serve as efficient quantum transducers, thanks to their strong intrinsic optical nonlinearities. This is primarily due to topologically enhanced optical responses, robust spin-orbit coupling, together with high spin density in MTIs. We demonstrate that unity transduction fidelity and GHz transduction bandwidth can be simultaneously achieved with modest experimental requirements, which can facilitate diverse applications in quantum information science and other fields.

Acknowledgment

We acknowledge support from Honda Research Institute USA.

References

[1] J. Verdú, H. Zoubi, C. Koller, J. Majer, H. Ritsch, and J. Schmiedmayer, *Strong Magnetic Coupling of an Ultracold Gas to a Superconducting Waveguide Cavity*, Phys. Rev. Lett. **103**, 043603 (2009).

[2] M. Hafezi, Z. Kim, S. L. Rolston, L. A. Orozco, B. L. Lev, and J. M. Taylor, *Atomic Interface between Microwave and Optical Photons*, Phys. Rev. A - At. Mol. Opt. Phys. **85**, 020302 (2012).

[3] L. A. Williamson, Y.-H. Chen, and J. J. Longdell, *Magneto-Optic Modulator with Unit Quantum Efficiency*, Phys. Rev. Lett. **113**, 203601 (2014).

[4] C. O'Brien et al., *Interfacing Superconducting Qubits and Telecom Photons via a Rare-Earth-Doped Crystal*, Phys. Rev. Lett. **113**, 63603 (2014).

[5] M. Aspelmeyer, T. J. Kippenberg, and F. Marquardt, *Cavity Optomechanics*, Rev. Mod. Phys. **86**, 1391 (2014).

[6] R. W. Andrews, R. W. Peterson, T. P. Purdy, K. Cicak, R. W. Simmonds, C. A. Regal, and K. W. Lehnert, *Bidirectional and Efficient Conversion between Microwave and Optical Light*, Nat. Phys. 2014 104 **10**, 321 (2014).

[7] T. Bagci et al., *Optical Detection of Radio Waves through a Nanomechanical Transducer*, Nat. 2014 5077490 **507**, 81 (2014).

[8] M. Tsang, *Cavity Quantum Electro-Optics*, Phys. Rev. A - At. Mol. Opt. Phys. **81**, 063837 (2010).

[9] R. Hisatomi, A. Osada, Y. Tabuchi, T. Ishikawa, A. Noguchi, R. Yamazaki, K. Usami, and Y. Nakamura, *Bidirectional Conversion between Microwave and Light via Ferromagnetic Magnons*, Phys. Rev. B **93**, 174427 (2016).

[10] J. R. Everts, M. C. Berrington, R. L. Ahlefeldt, and J. J. Longdell, *Microwave to Optical Photon Conversion via Fully Concentrated Rare-Earth-Ion Crystals*, Phys. Rev. A **99**, 063830 (2019).

[11] M. H. Devoret and R. J. Schoelkopf, *Superconducting Circuits for Quantum Information: An Outlook*, Science (80-.). **339**, 1169 (2013).

[12] M. Saffman, T. G. Walker, and K. Mølmer, *Quantum Information with Rydberg Atoms*, Rev. Mod. Phys. **82**, 2313 (2010).

[13] A. K. Hamze, M. Reynaud, J. Geler-Kremer, and A. A. Demkov, *Design Rules for Strong Electro-Optic Materials*, Npj Comput. Mater. 2020 61 **6**, 1 (2020).

[14] Y. Xu, L. Elcoro, Z. Da Song, B. J. Wieder, M. G. Vergniory, N. Regnault, Y. Chen, C. Felser, and B. A. Bernevig, *High-Throughput Calculations of Magnetic Topological Materials*, Nat. 2020 5867831 **586**, 702 (2020).

[15] L. Elcoro, B. J. Wieder, Z. Song, Y. Xu, B. Bradlyn, and B. A. Bernevig, *Magnetic Topological Quantum Chemistry*, Nat. Commun. 2021 121 **12**, 1 (2021).

[16] Y. Deng, Y. Yu, M. Z. Shi, Z. Guo, Z. Xu, J. Wang, X. H. Chen, and Y. Zhang, *Quantum Anomalous Hall Effect in Intrinsic Magnetic Topological Insulator MnBi2Te4*, Science (80-.). **367**, 895 (2020).

[17] J. X. Qiu et al., *Axion Optical Induction of Antiferromagnetic Order*, Nat. Mater. 2023 225 **22**, 583 (2023).

[18] P. Němec, M. Fiebig, T. Kampfrath, and A. V. Kimel, *Antiferromagnetic Opto-Spintronics*, Nature Physics.

[19] J. Han, R. Cheng, L. Liu, H. Ohno, and S. Fukami, *Coherent Antiferromagnetic Spintronics*, Nat. Mater. 2023 1 (2023).

[20] P. Pirro, V. I. Vasyuchka, A. A. Serga, and B. Hillebrands, *Advances in Coherent Magnonics*, Nat. Rev. Mater. 2021 612 **6**, 1114 (2021).

[21] X. L. Qi and S. C. Zhang, *Topological Insulators and Superconductors*, Rev. Mod. Phys. **83**, 1057 (2011).

[22] M. Z. Hasan and C. L. Kane, *Colloquium: Topological Insulators*, Rev. Mod. Phys. **82**, 3045 (2010).

[23] H. Xu, J. Zhou, H. Wang, and J. Li, *Giant Photonic Response of Mexican-Hat Topological Semiconductors for Mid-Infrared to Terahertz Applications*, J. Phys. Chem. Lett. **11**, 6119 (2020).

[24] H. Xu, H. Wang, J. Zhou, Y. Guo, J. Kong, and J. Li, *Colossal Switchable Photocurrents in Topological Janus Transition Metal Dichalcogenides*, Npj Comput. Mater. **7**, 1 (2021).

[25] L. Z. Tan and A. M. Rappe, *Enhancement of the Bulk Photovoltaic Effect in Topological Insulators*, Phys. Rev. Lett. **116**, 237402 (2016).

[26] J. Shi et al., *Giant Room-Temperature Nonlinearities from a Monolayer Janus Topological Semiconductor*, (2023).

[27] J. Li, Y. Li, S. Du, Z. Wang, B. L. Gu, S. C. Zhang, K. He, W. Duan, and Y. Xu, *Intrinsic Magnetic Topological Insulators in van Der Waals Layered MnBi2Te4-Family Materials*, Sci. Adv. **5**, eaaw5685 (2019).

[28] D. Zhang, M. Shi, T. Zhu, D. Xing, H. Zhang, and J. Wang, *Topological Axion States in the Magnetic Insulator MnBi2Te4 with the Quantized Magnetoelectric Effect*, Phys. Rev. Lett. **122**, 206401 (2019).

[29] M. M. Otrokov et al., *Prediction and Observation of an Antiferromagnetic Topological Insulator*, Nature **576**, 416 (2019).
[30] K. Svensson et al., *Perspectives on Quantum Transduction*, Quantum Sci. Technol. **5**, 020501 (2020).
[31] J. Sipe and A. Shkrebtii, *Second-Order Optical Response in Semiconductors*, Phys. Rev. B **61**, 5337 (2000).
[32] M. Zgonik, P. Bernasconi, M. Duelli, R. Schlesser, P. Günter, M. H. Garrett, D. Rytz, Y. Zhu, and X. Wu, *Dielectric, Elastic, Piezoelectric, Electro-Optic, and Elasto-Optic Tensors of <math Xmlns="http://Www.W3.Org/1998/Math/MathML" Display="inline"><mrow><msub><mrow><mi Mathvariant="normal">BaTiO</Mi></Mrow><mrow><mn>3</Mn></Mrow></Msub></Mrow></Math> Crystals*, Phys. Rev. B **50**, 5941 (1994).
[33] K. D. Fredrickson, V. V. Vogler-Neuling, K. J. Kormondy, D. Caimi, F. Eltes, M. Sousa, J. Fompeyrine, S. Abel, and A. A. Demkov, *Strain Enhancement of the Electro-Optical Response in BaTi O3 Films Integrated on Si(001)*, Phys. Rev. B **98**, 075136 (2018).
[34] M. S. Dresselhaus, *SOLID STATE PHYSICS PART III Magnetic Properties of Solids* (n.d.).
[35] H. Xu, H. Wang, and J. Li, *Abnormal Nonlinear Optical Responses on the Surface of Topological Materials*, Npj Comput. Mater. **8**, 1 (2022).
[36] G. G. Scott, *Review of Gyromagnetic Ratio Experiments*, Rev. Mod. Phys. **34**, 102 (1962).
[37] Y. Ogata, H. Chudo, M. Ono, K. Harii, M. Matsuo, S. Maekawa, and E. Saitoh, *Gyroscopic g Factor of Rare Earth Metals*, Appl. Phys. Lett. **110**, (2017).
[38] D. Lujan et al., *Magnons and Magnetic Fluctuations in Atomically Thin MnBi2Te4*, Nat. Commun. 2022 131 **13**, 1 (2022).
[39] S. M. Rezende, A. Azevedo, and R. L. Rodriguez-Suarez, *Introduction to Antiferromagnetic Magnons*, J. Appl. Phys. **126**, 151101 (2019).
[40] H. Xu, H. Wang, J. Zhou, and J. Li, *Pure Spin Photocurrent in Non-Centrosymmetric Crystals: Bulk Spin Photovoltaic Effect*, Nat. Commun. 2021 121 **12**, 1 (2021).
[41] K. Batrakov, P. Kuzhir, S. Maksimenko, N. Volynets, S. Voronovich, A. Paddubskaya, G. Valusis, T. Kaplas, Y. Svirko, and P. Lambin, *Enhanced Microwave-to-Terahertz Absorption in Graphene*, Appl. Phys. Lett. **108**, 123101 (2016).
[42] L. M. Malard, T. V. Alencar, A. P. M. Barboza, K. F. Mak, and A. M. De Paula, *Observation of Intense Second Harmonic Generation from MoS2 Atomic Crystals*, Phys. Rev. B - Condens. Matter Mater. Phys. **87**, 201401 (2013).
[43] B. Li, D. M. Pajerowski, S. X. M. Riberolles, L. Ke, J. Q. Yan, and R. J. McQueeney, *Quasi-Two-Dimensional Ferromagnetism and Anisotropic Interlayer Couplings in the Magnetic Topological Insulator MnBi2Te4*, Phys. Rev. B **104**, L220402 (2021).
[44] L. M. Corliss, J. M. Hastings, R. Nathans, and G. Shirane, *Magnetic Structure of Cr2O3*, J. Appl. Phys. **36**, 1099 (1965).
[45] R. Fei, W. Song, and L. Yang, *Giant Linearly-Polarized Photogalvanic Effect and Second Harmonic Generation in Two-Dimensional Axion Insulators*, (2020).
[46] H. Wang and X. Qian, *Electrically and Magnetically Switchable Nonlinear Photocurrent in PT-Symmetric Magnetic Topological Quantum Materials*, Npj Comput. Mater. 2020 61 **6**, 1 (2020).
[47] Q. Ma, R. Krishna Kumar, S. Y. Xu, F. H. L. Koppens, and J. C. W. Song, *Photocurrent as a Multiphysics Diagnostic of Quantum Materials*, Nat. Rev. Phys. 2023 53 **5**, 170 (2023).
[48] A. I. Lvovsky, *Squeezed Light*, Photonics Sci. Found. Technol. Appl. **1**, 121 (2015).
[49] R. Sahu, L. Qiu, W. Hease, G. Arnold, Y. Minoguchi, P. Rabl, and J. M. Fink, *Entangling Microwaves with Light*, Science (80-.). **380**, 718 (2023).
[50] H. Y. Yuan, P. Yan, S. Zheng, Q. Y. He, K. Xia, and M. H. Yung, *Steady Bell State Generation via Magnon-Photon Coupling*, Phys. Rev. Lett. **124**, (2020).
[51] S. Probst, H. Rotzinger, S. Wünsch, P. Jung, M. Jerger, M. Siegel, A. V. Ustinov, and P. A. Bushev, *Anisotropic Rare-Earth Spin Ensemble Strongly Coupled to a Superconducting Resonator*, Phys. Rev. Lett. **110**, 157001 (2013).
[52] M. J. Collett and C. W. Gardiner, *Squeezing of Intracavity and Traveling-Wave Light Fields Produced in Parametric Amplification*, Phys. Rev. A **30**, 1386 (1984).
[53] J. P. Covey, A. Sipahigil, and M. Saffman, *Microwave-to-Optical Conversion via Four-Wave Mixing in a Cold Ytterbium Ensemble*, Phys. Rev. A **100**, 012307 (2019).
[54] Y. Reshitnyk, M. Jerger, and A. Fedorov, *3D Microwave Cavity with Magnetic Flux Control and Enhanced Quality Factor*, EPJ Quantum Technol. **3**, 1 (2016).
[55] C. Lecaplain, C. Javerzac-Galy, M. L. Gorodetsky, and T. J. Kippenberg, *Mid-Infrared Ultra-High-Q Resonators Based on Fluoride Crystalline Materials*, Nat. Commun. 2016 71 **7**, 1 (2016).
[56] J. Han, T. Vogt, C. Gross, D. Jaksch, M. Kiffner, and W. Li, *Coherent Microwave-to-Optical*

Conversion via Six-Wave Mixing in Rydberg Atoms, Phys. Rev. Lett. **120**, 093201 (2018).
[57] F. Sedlmeir et al., *Efficient Microwave to Optical Photon Conversion: An Electro-Optical Realization*, Opt. Vol. 3, Issue 6, Pp. 597-604 **3**, 597 (2016).
[58] C. Couteau, *Spontaneous Parametric Down-Conversion*, Https://Doi.Org/10.1080/00107514.2018.1488463 **59**, 291 (2018).
[59] Q. Guo et al., *Ultrathin Quantum Light Source with van Der Waals NbOCl2 Crystal*, Nat. 2023 6137942 **613**, 53 (2023).